Modal Control of Piezolaminated Anisotropic Rectangular Plates Part 2: Control Theory

Scott E. Miller,* Yaakov Oshman,[†] and Haim Abramovich[‡]

Technion—Israel Institute of Technology, Haifa 32000, Israel

A general selective modal control design methodology is presented for piezolaminated anisotropic plate systems that utilizes selective modal transducers to realize any number of possible modal control strategies. A selective modal control design procedure is specified that defines a step-by-step framework through which the structural and control subdesign processes are effectively integrated. Several conditions that sufficiently ensure asymptotic stability are derived and then discussed in the context of deriving selective modal control methods that are stability robust to modeling and implementation errors. Several selective modal control examples are then given in which selective modal transducers are designed and control laws chosen so as to allow for 1) the contributions of any given mode to the active energy extraction rate to be directly specified and 2) pole locations to be selectively and dynamically varied or 3) both pole locations and selective modal transducer design constants to be optimally determined. A numerical example is presented in which a stability-robust optimal selective modal control method is developed for a cantilevered anisotropic plate. Maintaining a linear feedback law, a single self-sensing selective modal transducer is employed whose design parameters were chosen to optimize the system response to a given initial excitation. Frequency and transient response analyses show a dramatic enhancement in system performance and accurately concur with theoretical predictions. The example serves both to illustrate the design process and to independently validate selective modal transducer and selective modal control theoretical results.

I. Introduction

WITHIN the past decade several vibration control techniques have been developed for simple beam and plate systems that utilize distributed piezoelectric transducers formed from polyvinylidine fluoride (PVDF). PVDF actuators have been designed whose spatially varying piezoelectric field properties were exploited to provide for the simultaneous control of all modes or special modal subsets in cantilevered and simply supported beams.[1,2] Miller and Hubbard[3] developed a reciprocal sensor theory and subsequently incorporated PVDF sensors and actuators into multicomponent systems in which each component itself was a smart structural member. Burke and Hubbard[4] developed a formulation for the control of thin elastic (Kirchhoff–Love) isotropic plates subject to most combinations of free, clamped, or pinned boundary conditions, in which the active elements were spatially varying biaxially polarized piezoelectric transducer layers. Lee[5] generalized the classical laminate plate theory to include the effect of laminated piezoelectric layers and, thus, to provide a theoretical framework for the distributed transduction of bending, torsion, shearing, shrinking, and stretching in flexible anisotropic plates. Miller et al.[6] subsequently employed Lyapunov's second method to derive a general active vibration suppression control design methodology for anisotropic laminated piezoelectric plates.

As was discussed in our companion paper,[7] the aforementioned vibration control strategies share several common limitations. Perhaps most significantly, although all of these methods reduce the vibration control task to a selection of individual piezolaminae field functions, none offer a general method for determining those field functions so as to ensure active vibration suppression. Therefore, a clearly defined design methodology is developed herein in which the structural and control design processes are integrated to yield a framework for truly selective modal control (SMC). A broad class

of stability robust SMC approaches is defined through the identification of conditions that sufficiently ensure global asymptotic stability without requiring perfect knowledge of design parameters, structural constants, or modal behavior. Specific SMC design examples are given that allow for 1) the contributions of any given mode to the active energy extraction rate to be directly specified and 2) pole locations to be selectively and dynamically varied or 3) pole locations, selective modal transducer (SMT) design parameters, and feedback laws to be optimally determined. The SMC design approach is illustrated through a numerical example involving a piezolaminated anisotropic plate. The stability robust, single input/single output type, optimal design that emerges serves to verify the major theoretical conclusions presented in both Parts 1 and 2 of this work.

II. System Description

Figure 1 describes the geometry of the general system under consideration. A rectangular anisotropic plate with exactly N piezoelectrically active laminate layers is considered. Contrary to what may be implicitly assumed from the figure, transducer layers may be located anywhere in the structure. The length dimensions of the system in the x and y directions are denoted L_a and L_b, respectively. Each piezoelectric layer may be independently anisotropic, and its electromechanical field strength may be selectively varied in both spatial dimensions. The material properties within each lamina are assumed continuous. A complete system description may be found in Part 1.
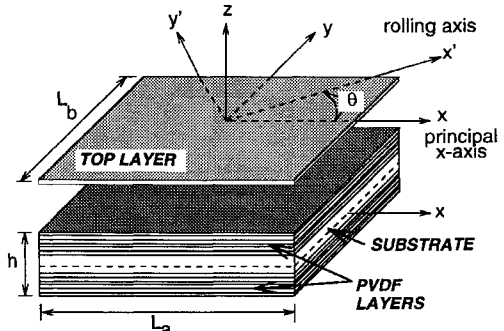
Fig. 1 Geometry of general piezoelectric laminate system.

Applying the well-known Kirchhoff–Love approximation, the equations of motion of the general system described in Fig. 1 were developed in Part 1 and are expressed in the form

$$x_{tt} + Cx_t + \mathcal{K}x = -\frac{1}{\rho h} \mathcal{D}' \left(\sum_{k=1}^{N} e_0^k \Lambda^k V^k \right) \qquad (1)$$

where

$$\mathcal{D} \triangleq \begin{bmatrix} \frac{\partial}{\partial x} & \frac{\partial}{\partial y} & 0 & 0 & 0 & 0 \\ 0 & \frac{\partial}{\partial x} & \frac{\partial}{\partial y} & 0 & 0 & 0 \\ 0 & 0 & 0 & \frac{\partial^2}{\partial x^2} & 2\frac{\partial^2}{\partial x \partial y} & \frac{\partial^2}{\partial y^2} \end{bmatrix}' \qquad (2)$$

$$\mathcal{E} \triangleq \begin{bmatrix} -\frac{\partial}{\partial x} & -\frac{\partial}{\partial y} & 0 & 0 & 0 & 0 \\ 0 & -\frac{\partial}{\partial x} & -\frac{\partial}{\partial y} & 0 & 0 & 0 \\ 0 & 0 & 0 & \frac{\partial^2}{\partial x^2} & 2\frac{\partial^2}{\partial x \partial y} & \frac{\partial^2}{\partial y^2} \end{bmatrix}' \qquad (3)$$

$$\mathcal{K} \triangleq (1/\rho h) \mathcal{D}' K_a \mathcal{E} \qquad (4)$$

$$\mathcal{C} \triangleq b_0 \mathcal{I} + c_0 \mathcal{K} \qquad (5)$$

$$x \triangleq [u \quad v \quad w]' \qquad (6)$$

$$K_a \triangleq \begin{bmatrix} A_{11} & A_{16} & A_{12} & B_{11} & B_{16} & B_{12} \\ A_{16} & A_{66} & A_{26} & B_{16} & B_{66} & B_{26} \\ A_{12} & A_{26} & A_{22} & B_{12} & B_{26} & B_{22} \\ B_{11} & B_{16} & B_{12} & D_{11} & D_{16} & D_{12} \\ B_{16} & B_{66} & B_{26} & D_{16} & D_{66} & D_{26} \\ B_{12} & B_{26} & B_{22} & D_{12} & D_{26} & D_{22} \end{bmatrix} \qquad (7)$$

A_{ij}, B_{ij}, and D_{ij} are the constitutive material constants that characterize the mechanical stress–strain behavior of the composite system. The constants b_0 and c_0 are viscous and structural damping coefficients, respectively, whereas $\mathcal{I}$ is the identity operator. $V^k = V^k(t)$ is the spatially independent driving voltage applied across the kth piezolamina. The electromechanical field strength of each piezolamina is described mathematically via the product $e_0^k \Lambda^k$, where Λ^k is a dimensionless and spatially varying piezoelectric field distribution function and $e_0^k \in \mathfrak{R}^6$ is a vector of piezoconstants relative to the point of maximum electromechanical transduction.

The boundary conditions as derived in Part 1 are stated in Table 1, where the in-plane resultant forces $(N \triangleq [N_1 \ N_6 \ N_2]')$ and moments $(M \triangleq [M_1 \ M_6 \ M_2]')$ are given by

$$\begin{bmatrix} N \\ M \end{bmatrix} = -K_a \mathcal{E}x - \sum_{k=1}^{N} e_0^k \Lambda^k V^k \qquad (8)$$

and the transverse shear force resultants Q_1 and Q_2 are defined as

$$(Q_1) = [(M_1)]_x + [(M_6)]_y \qquad (9)$$

$$(Q_2) = [(M_6)]_x + [(M_2)]_y \qquad (10)$$

Finally, the current accumulated on the surface electrode of the kth lamina because of the mechanical displacement of the laminates was determined in Part 1:

$$i^k(t) = -\iint_A (\mathcal{E}x_t)' e_0^k \Lambda^k \, dA \qquad (11)$$

Table 1 Boundary conditions

$x = -(L_a/2, L_a/2)$	$y = -(L_b/2, L_b/2)$
(N_1) or u	(N_2) or v
(N_6) or v	(N_6) or u
(Q_1) or w	(Q_2) or w
(M_1) or w_x	(M_2) or w_y
(M_6) or w_y	(M_6) or w_x

III. SMC

A. General Definition

The SMTs developed in Part 1 may be used to implement a number of modal control strategies for composite plates in which both the SMT design and control law are chosen to optimize or else prespecify the dynamic response of a targeted modal subset. These SMC strategies may be designed so as to guarantee asymptotic stability regardless of errors that occur in the design process. Moreover, the freedom to arbitrarily determine SMT behavior as part of the design process typically leads to enhanced system performance and reduced burden on the control law itself.

It was shown in Part 1 that if specific criteria (henceforth called SMT construct conditions) regarding the location, orientation, number, and electromechanical transduction of piezosublaminae are obeyed then the SMT design process allows for the equations of motion [Eq. (1)] to be reduced to the form

$$\ddot{q}_m + (b_0 + c_0\lambda)\dot{q}_m + \lambda_m q_m = -\alpha_m \lambda_m V_a(t) \qquad m = 1, 2, \ldots \qquad (12)$$

where λ_m, $q_m(t)$, and α_m are the eigenvalue, generalized modal coordinate, and designer-specified modal participation factor (MPF) associated with the mth mode, respectively. The SMT driving voltage is referred to as $V_a(t)$. The preceding SMT actuator equation is complemented by the following SMT sensor equation:

$$i_s(t) = -\rho h \sum_{j=1}^{\infty} \beta_j \lambda_j \dot{q}_j(t) \qquad (13)$$

where β_j is the (sensor) MPF associated with the jth mode. When Eqs. (12) and (13) are realized via the same set of piezosublaminae,[8,9] $\alpha_j = \beta_j$ and the SMT is called a self-sensing selective modal actuator (SSMA). When functioning as dedicated selective modal actuators (SMAs) or selective modal sensors (SMSs), SMTs are henceforth referred to as SMAs or SMSs.

The system description may be further generalized to include the possibility of multiple SMTs. Assuming that each SMT requires exactly N piezosublaminae and assuming the existence of exactly p dedicated SMAs and q dedicated SMSs, the general equation of motion of the form

$$x_{tt} + Cx_t + \mathcal{K}x = -\frac{1}{\rho h} \mathcal{D}' \left(\sum_{k=1}^{p \cdot N} e_0^k \Lambda^k V^k \right) \qquad (14)$$

is reduced via the SMT construct conditions (see Theorem 1, Part 1) to

$$\ddot{q}_m + (b_0 + c_0\lambda)\dot{q}_m + \lambda_m q_m = -\sum_{l=1}^{p} \alpha_m^l \lambda_m V_a^l(t) \qquad (15)$$

whereas the q SMS output equations become (via Theorem 3, Part 1)

$$i_s^n(t) = -\rho h \sum_{j=1}^{\infty} \beta_j^n \lambda_j \dot{q}_j(t), \qquad n \in [1, 2, \ldots, q] \qquad (16)$$

where the driving voltage of the lth SMA ($l \in [1, \ldots, p]$) is referred to as $V_a^l(t)$ and the measured current of the nth SMS ($n \in [1, \ldots, q]$) as $i_s^n(t)$. If the lth SMA is self-sensing (i.e., an SSMA) then, for some $n \in [1, \ldots, q]$, $l = n$ and $\beta_j^n = \alpha_j^l$ for all j. Note that the mth mode is controllable only if at least one $\alpha_m^l \neq 0$ for some $l \in [1, \ldots, p]$ and observable only if at least one $\beta_m^l \neq 0$ for some $l \in [1, \ldots, q]$. Let R be an r-dimensional subset of modes targeted for active control. Since $\alpha_m^l, \beta_m^n = 0 \, \forall m \notin R$, then from Eqs. (15)

and (16) each excluded mode is completely decoupled from all other modes and, hence, will not lead to spillover in any active control strategy based solely on the targeted subset. Considering only the r modes in R, Eqs. (15) and (16) may be constructed in the form

$$\frac{d}{dt}\begin{bmatrix} q_1 \\ \vdots \\ q_r \\ \overline{\dot{q}_1} \\ \vdots \\ \dot{q}_r \end{bmatrix}$$

$$= \begin{bmatrix} 0 & & & 1 & & \\ & \ddots & & & \ddots & \\ & & 0 & & & 1 \\ \hline -\lambda_1 & & & -(b_0 + c_0\lambda_1) & & \\ & \ddots & & & \ddots & \\ & & -\lambda_r & & & -(b_0 + c_0\lambda_r) \end{bmatrix}$$

(17)

$$\times \begin{bmatrix} q_1 \\ \vdots \\ q_r \\ \overline{\dot{q}_1} \\ \vdots \\ \dot{q}_r \end{bmatrix} + \begin{bmatrix} 0 & & \\ & \ddots & \\ & & 0 \\ \hline -\alpha_1^1\lambda_1 & \cdots & -\alpha_1^p\lambda_1 \\ \vdots & \ddots & \vdots \\ -\alpha_r^1\lambda_r & \cdots & -\alpha_r^p\lambda_r \end{bmatrix} \begin{bmatrix} V_a^1 \\ \vdots \\ V_a^p \end{bmatrix}$$

$$\begin{bmatrix} \frac{i_s^1}{\rho h} \\ \vdots \\ \frac{i_s^q}{\rho h} \end{bmatrix} = \begin{bmatrix} 0 & & & -\beta_1^1\lambda_1 & \cdots & -\beta_r^1\lambda_r \\ & \ddots & & \vdots & \ddots & \vdots \\ & & 0 & -\beta_1^q\lambda_1 & \cdots & -\beta_r^q\lambda_r \end{bmatrix} \begin{bmatrix} q_1 \\ \vdots \\ q_r \\ \overline{\dot{q}_1} \\ \vdots \\ \dot{q}_r \end{bmatrix}$$

or, in abbreviated notation,

$$\dot{x}_a = A x_a + \begin{bmatrix} 0 \\ -\alpha \end{bmatrix} V, \qquad i = [0 \quad -\beta'] x_a \qquad (18)$$

where $x_a' \triangleq [q_a' \quad \dot{q}_a']'$ and the matrix definitions are obvious. For convenience the output vector i contains the q SMS current outputs normalized relative to ρh. The matrices $\alpha \in \mathfrak{R}^{r,p}$ and $\beta \in \mathfrak{R}^{r,q}$ are defined such that if the kth SMA is self-sensing then the kth columns of α and β are identical. If all SMAs are self-sensing (and no dedicated SMSs exist), $\alpha = \beta$.

SMC is realized when the matrices α, β, and a control law of the general form $V = V(i)$ are established so as to best satisfy a given performance objective. Design parameters may be chosen either directly or else through the optimization of a general performance index of the form $\mathcal{J} = \mathcal{J}(x_a, \alpha, \beta)$. In general terms, the SMC design procedure evolves through the following process: 1) A composite plate structural design is determined to satisfy the mechanical requirements (mass, stiffness, fabrication complexity, etc.). 2) The structure is modeled. 3) A suitable performance objective is established; Eq. (18) is acquired based on the r modes targeted for active control and then used to determine a suitable control law and selection of MPFs. 4) The design is assessed and, if no further reiteration is required, the piezofield functions (Λ_l^k) for each piezolamina are determined via Eq. (30), Part 1. The design is then implemented physically. Some of these steps are now briefly considered.

1. Structural Design

The process of satisfying structural requirements will necessarily dictate the number of piezolaminae to be incorporated, and hence the number of available SMTs. The structure must be designed such that all SMT (geometric) construct conditions are satisfied (Conditions C1–C5, Part 1): hence, six laminae per anisotropic plate SMT are

required (orthotropic and isotropic plates require fewer layers) with some imposed restrictions regarding skew angles. From a control standpoint the advantage of multiple SMTs may be small, as many control design objectives are likely to be sufficiently attainable even via a single SSMA.

2. Performance Objective

Having obtained a satisfactory representation of Eq. (18), performance objectives must be determined that will dictate the dynamic character of the actively controlled plate as well as the stability robustness of the system to errors that will inevitably occur during the modeling and implementation phases. The consequence of such errors is that the field distribution functions (Λ_k^l, Λ_k^n) that are ultimately implemented will lead to an imperfect realization of the MPFs (residing in α and β) specified as the outcome of the design process. Higher order modes whose MPFs were theoretically set to zero are likely, in final implementation, to possess nonzero MPFs. Stability robustness is, therefore, assessed in terms of the sensitivity of a given design to errors in α and β as $r \to \infty$. In the sections that immediately follow, criteria are determined to assess the stability robustness of a given design and a number of representative performance objectives are discussed.

B. Stability Robust SMC

In this section, sufficient conditions that ensure asymptotic stability are developed and then discussed in the context of stability robustness. Letting $k \in [1, \ldots, N]$ and $l \in [1, \ldots, p]$, it is convenient to associate each of the $p \cdot N$ actuator laminae with unique indices k and l. The (k, l) piezolamina is then uniquely associated with a driving voltage $V_k^l(t)$, piezofield function Λ_k^l, and piezoproperty vector $(e_0)_k^l$. Each of the dedicated $q \cdot N$ sensor laminae may be likewise assigned an indexed pair (k, n) ($n \in [1, \ldots, q]$) and associated with Λ_k^n, $(e_0)_k^n$, and a measured current $i_k^n(t)$ given by Eq. (11). If the (k, l) layer is self-sensing, then the (k, l) and (k, n) piezolaminae are identical for some $n \in [1, \ldots, q]$. The following postulate is then introduced.

Postulate 1: Consider an anisotropic rectangular plate containing at least $p \cdot N$ piezolaminae whose equations of motion are given by Eq. (14). Then, if the entire set of control inputs $\{V_k^l(t)\}_{k=1,\ldots,N}^{l=1,\ldots,p}$ satisfy

$$\sum_{l=1}^p \sum_{k=1}^N V_k^l(t) \iint_A (\mathcal{E}x_t)'(e_0)_k^l \Lambda_k^l \, dA \geq 0 \qquad (19)$$

the closed-loop system is asymptotically stable.

Proof: Consider the following (positive definite) Lyapunov functional:

$$J = \frac{1}{2} \iint_A [\rho h x_t' x_t + (\mathcal{E}x)' K_a(\mathcal{E}x)] \, dA \qquad (20)$$

whose first and second terms in the integrand, respectively, represent the kinetic and mechanical strain energy states.[10] The functional time derivative is then

$$\dot{J} = \iint_A [\rho h x_t' x_{tt} + (\mathcal{E}x_t)' K_a(\mathcal{E}x)] \, dA \qquad (21)$$

Substituting Eq. (8) into the preceding expression (with modified double index notation) yields

$$\dot{J} = \iint_A \left\{ \rho h x_t' x_{tt} - (\mathcal{E}x_t)' \begin{bmatrix} N \\ M \end{bmatrix} \right\} dA$$

$$- \sum_{l=1}^p \sum_{k=1}^N V_k^l \iint_A (\mathcal{E}x_t)'(e_0)_k^l \Lambda_k^l \, dA \qquad (22)$$

Integrating the first term of Eq. (22) by parts,

$$\dot{J} = \iint_A \left\{ \rho h x_t' \left(x_{tt} - \frac{1}{\rho h} \mathcal{D}' \begin{bmatrix} N \\ M \end{bmatrix} \right) \right\} dA$$

$$- \sum_{l=1}^p \sum_{k=1}^N V_k^l \iint_A (\mathcal{E}x_t)'(e_0)_k^l \Lambda_k^l \, dA + I_3 + I_4 \qquad (23)$$

where I_3 and I_4 are the line integrals

$$I_3 = \int_{-L_b/2}^{L_b/2} \{N_1 u_t + N_6 v_t + Q_1 w_t$$

$$- M_1 w_{xt} - M_6 w_{yt}\}_{x=-L_a/2}^{x=L_a/2} \, dy \tag{24}$$

$$I_4 = \int_{-L_a/2}^{L_a/2} \{N_6 u_t + N_2 v_t + Q_2 w_t$$

$$- M_6 w_{xt} - M_2 w_{yt}\}_{y=-L_b/2}^{y=L_b/2} \, dx \tag{25}$$

It is obvious that both of the preceding integrals vanish for any possible set of boundary conditions admitted in Table 1. Combining Eqs. (1), (4), and (8) with Eq. (23) and dismissing the boundary integrals leads to the result

$$\dot{J} = -\rho h \iint_A \dot{x}_t' C x_t \, dA$$

$$- \sum_{l=1}^{p} \sum_{k=1}^{N} V_k^l \iint_A (\mathcal{E} x_t)'(e_0)_k^l \Lambda_k^l \, dA \tag{26}$$

According to the second method of Lyapunov, the system is asymptotically stable if $\dot{J}$ is negative definite. Realize that Eq. (26) is synonymous with energy flux and that only the second term on the right-hand side (RHS) of the equation contains the influence of the piezoelectric layers. The first term represents the energy flux inherent to the passive system. It was established in Part 1 that the operator C is positive definite for all systems under study except for those exhibiting rigid body motions in a perfectly vacuous environment. (In such a case, however, a flexible modal subsystem may be derived whose damping operator C is nonetheless positive definite.[6]) Excluding this special case, the first term is always dissipative (i.e., negative definite): hence, the system will be asymptotically stable as long as the piezoelectrically induced forces do not add energy to the system. Asymptotic stability is then contingent on the negative semidefiniteness of $\dot{J}_p$, where

$$\dot{J}_p \triangleq - \sum_{l=1}^{p} \sum_{k=1}^{N} V_k^l \iint_A (\mathcal{E} x_t)'(e_0)_k^l \Lambda_k^l \, dA \tag{27}$$

which is the condition stated in the postulate.   □

Remark: The expression

$$\iint_A (\mathcal{E} x_t)'(e_0)_k^l \Lambda_k^l \, dA$$

is equivalent to the measurement obtained from the (k, l) piezolamina when functioning as a self-sensing actuation layer [Eq. (11)]. Hence, in this special case

$$\dot{J}_p = \sum_{l=1}^{p} \sum_{k=1}^{N} V_k^l(t) i_k^l(t) \tag{28}$$

which lends itself to an intuitive explanation: the contribution to the total energy flux (i.e., power) because of the active electromechanical transduction is the total sum of electrical power associated with each individual layer. It also indicates that asymptotic stability is automatically ensured if each layer is self-sensing and the control input to each layer is any function opposite in sign to the measured current.

Postulate 1 may be used to establish a criterion for asymptotic stability that is central to the development of stability robust SMC. Defining $q_a \triangleq [q_1, \ldots, q_r]'$, see Theorem 1.

Theorem 1: Consider an anisotropic rectangular plate containing p SMAs whose equations of motion are given by Eq. (18). Then, if $V = V(\dot{q}_a)$ is such that $\dot{q}_a' \alpha V \geq 0$, the closed-loop system is asymptotically stable.

Proof: A required SMA construct condition is that $V_k^l(t) = (g_0)_k^l V_a^l(t)$ (Part 1, Theorem 1). Hence, Eq. (27) becomes

$$\dot{J}_p \triangleq - \sum_{l=1}^{p} V_a^l \sum_{k=1}^{N} \iint_A (\mathcal{E} x_t)'(g_0)_k^l (e_0)_k^l \Lambda_k^l \, dA \tag{29}$$

Theorem 3, Part 1, establishes that

$$\sum_{k=1}^{N} \iint_A (\mathcal{E} x_t)'(g_0)_k^l (e_0)_k^l \Lambda_k^l \, dA = \rho h \sum_{j=1}^{r} \alpha_j^l \lambda_j \dot{q}_j(t) \tag{30}$$

Substituting Eq. (30) into Eq. (29) and expressing the result in matrix form,

$$\dot{J}_p = -\rho h (\dot{q}_a' \alpha V) \tag{31}$$

the negative semidefiniteness of which is ensured by the condition stated in the theorem.   □

Several corollaries of Theorem 1 are now established. Denoting the element by element Schur product of two matrices A and B as $A \circ B$ and defining $\text{sgn}(i) \triangleq [\text{sgn}(i_s^1/\rho h) \cdots \text{sgn}(i_s^q/\rho h)]'$, see the following corollary.

Corollary 1: Consider an anisotropic rectangular plate containing $p = q$ self-sensing SMAs such that $\alpha = \beta$ in Eq. (18). Then, if $V = -g(t) \circ \text{sgn}(i)$ for any arbitrary function $g(t) \in \Re^p$ with only nonnegative elements, the closed-loop system is asymptotically stable.

Proof: If $\alpha = \beta$ then $i = -\alpha' \dot{q}_a$ [Eq. (18)]. Hence, in this special case, $\dot{J}_p = \rho h V' i$ is negative semidefinite (NSD) if $V = -g(t) \circ \text{sgn}(i)$.   □

The following corollaries pertain to linearly derived formulations of $V(\dot{q}_a)$.

Corollary 2: Consider an anisotropic rectangular plate containing p SMAs and q SMSs whose equations of motion are given by Eq. (18). Let $V = -G(t)i$ for any arbitrary $G \in \Re^{p,q}$. Then, if α and β are such that $(\alpha G \beta') \in \Re^{r,r}$ is positive semidefinite, the closed-loop system is asymptotically stable.

Proof: Substituting $V = -G(t)i$ into Eq. (31) and then applying Eq. (18) yields $\dot{J}_p = -\rho h [\dot{q}_a'(\alpha G \beta') \dot{q}_a]$, which is NSD for any positive semidefinite (PSD) $\alpha G \beta'$.   □

Corollary 3: Consider an anisotropic rectangular plate containing p self-sensing SMAs such that $\alpha = \beta$ in Eq. (18). Let $V = -G(t)i$ for any arbitrary $G \in \Re^{p,p}$. Then, if G is positive semidefinite, the closed-loop system is asymptotically stable.

Proof: If $\alpha = \beta$ then $i = -\alpha' \dot{q}_a$ [Eq. (18)]. Then from Eq. (31),

$$\dot{J}_p = -\rho h [\dot{q}_a'(\alpha G \alpha') \dot{q}_a] = -\rho h [i' G i] \tag{32}$$

which is NSD only if G is PSD.   □

Corollary 4: Consider an anisotropic rectangular plate containing p SMAs and q SMSs whose equations of motion are given by Eq. (18). Let $\min(p, q) = 1$ and let $V = -G(t)i$ for any arbitrary $G \in \Re^{p,q}$. Then, if all elements of α, β, and G are nonnegative, the closed-loop system is asymptotically stable.

Proof: If $p = 1$ or $q = 1$ then rank $(\alpha G \beta') = 1$ and thus $\alpha G \beta'$ has at most one nonzero eigenvalue.[11] Since $\text{tr}(\alpha G \beta')$ is equal to that nonzero eigenvalue, all eigenvalues of $\alpha G \beta'$ are nonnegative if $\text{tr}(\alpha G \beta') \geq 0$. All eigenvalues are thus nonnegative if all elements of α, β, and G are likewise nonnegative, in which case $[\alpha G \beta']$ is PSD. Asymptotic stability is established via Corollary 2.   □

Theorem 1 and its corollaries establish the five cases given in Table 2. Case 1 is the most general of all cases listed, and it will be difficult to use the associated stability criterion to assess stability robustness. Cases 2 and 4 show that as long as $\alpha = \beta$ as $r \to \infty$ then asymptotic stability is guaranteed provided that, respectively, $V = -g(t) \circ \text{sgn}(i)$ or $V = -Gi$ for any PSD gain matrix G. If i is entirely derived via p self-sensing SMAs, then $\alpha = \beta$ is essentially ensured even when modeling and implementation errors yield MPFs that differ somewhat from those specified as the outcome of the design process. Case 3 is the most general linear scenario: stability robustness is assessed through determining the sensitivities of the eigenvalues of $\alpha G \beta'$ to perturbations in α and β. A parameter space may be determined (or bounded) that defines the entire set of

Table 2   Stability criteria case study

Case	MPFs	$\min(p, q)$	Control law	Criterion
1	$\alpha \neq \beta$	≥ 1	$V = V(\dot{q}_a)$	$\dot{q}_a' \alpha V \geq 0$
2	$\alpha = \beta$	≥ 1	$V = V(i)$	$V = -g(t) \circ \text{sgn}(i)$
3	$\alpha \neq \beta$	≥ 1	$V = -Gi$	$\alpha G \beta' \geq 0$
4	$\alpha = \beta$	≥ 1	$V = -Gi$	$G \geq 0$
5	$\alpha \neq \beta$	1	$V = -Gi$	elements $\alpha, \beta, G \geq 0$

admissible α and β for which all eigenvalues remain nonnegative. In case 5 asymptotic stability is sufficiently ensured when α and β are composed entirely of nonnegative elements. Asymptotic stability is obviously possible even if this condition is violated (as long as $\alpha G \beta'$ is PSD), but the condition itself may possibly be verified on an actual structure through an experimental test: each targeted mode may be excited individually and the sign of each specific modal participation factor determined. It is obvious that stability robustness is most easily ensured (virtually automatically) through either the case 2 or case 4 configurations.

C.   Representative Performance Objectives

1.   Nonlinear Selective Energy Extraction

Several possible performance objectives are now explored. In this first example, a nonlinear SMC method is derived (i.e., α, β, and a control law are determined) whose objective is to explicitly define the contribution of each mode to the active energy extraction rate. The case 2 (Table 2) stability criteria are imposed so as to ensure a stability robust design: hence, $\alpha = \beta$ and the control law is $V = -g(t) \circ \text{sgn}(i)$. Recalling that $i = -\alpha' \dot{q}_a$ [via Eq. (16)], the control law becomes

$$V = -g(t) \circ \text{sgn}(i) = \left[g^1(t) \text{sgn} \left(\sum_{j=1}^{r} \alpha_j^1 \lambda_j \dot{q}_j \right) \right.$$

$$\left. \cdots g^P(t) \text{sgn} \left(\sum_{j=1}^{r} \alpha_j^p \lambda_j \dot{q}_j \right) \right]' \qquad (33)$$

where $g^l(t)$ is the lth (nonnegative) element of $g(t)$. Substituting Eq. (33) into Eq. (31), the energy flux may be expressed in the form

$$\dot{J}_p = -\rho h \sum_{l=1}^{p} g^l(t) \left| \sum_{j=1}^{r} \alpha_j^l \lambda_j \dot{q}_j(t) \right| \qquad (34)$$

The character of the energy extraction rate may then be specifically determined by the arbitrarily chosen elements of $g(t) \in \mathfrak{R}^p$. Two special cases are worth mentioning: if $p = 1$ and $g(t) = 1$, then

$$\dot{J}_p = -\rho h \left| \sum_{j=1}^{r} \alpha_j \lambda_j \dot{q}_j(t) \right| \qquad (35)$$

whereas if $p = r, g(t) = [1 \cdots 1]'$, and $\alpha_j^l = \alpha_j \delta_{jl}$ (where δ_{jl} is the Kroenecker delta function), then

$$\dot{J}_p = -\rho h \sum_{j=1}^{r} |\alpha_j \lambda_j \dot{q}_j(t)| \qquad (36)$$

From a structural point of view, Eq. (35) is the simplest possible case (only a single SMT is required) whereas Eq. (36) is the most complex (one SMT per mode). Nonetheless Eq. (36), unlike Eq. (35), avoids the existence of nontrivial state trajectories for which $\dot{J}_p = 0$ and, hence, guarantees active energy extraction along any trajectory.

2.   Linear Selective Energy Extraction

When the case 3 (Table 2) scenario is obeyed so that the control law is $V = -Gi$, then the energy flux expression [Eq. (31)] becomes

$$\dot{J}_p = -\rho h [\dot{q}_a'(\alpha G \beta') \dot{q}_a] \qquad (37)$$

from which an energy-based linear method may be derived. The performance objective is to select α, β, and $G(t)$ to maximize the

energy extracted from each targeted mode relative to a specified weighting. The control law transforms Eq. (18) into the (closed-loop) system equation

$$\dot{x}_a = A_a x_a, \qquad A_a \triangleq A - \begin{bmatrix} 0 & 0 \\ 0 & -\alpha G \beta' \end{bmatrix} \qquad (38)$$

Integrating Eq. (37) over the time interval $t = [0, t_f]$, the total energy that is actively added to the system via the piezoelectric laminae is then

$$J_p = -\rho h \int_0^{t_f} [\dot{q}_a'(\alpha G \beta') \dot{q}_a] \, dt \qquad (39)$$

Introducing an arbitrarily specified state weighting matrix, $\bar{Q} \in \mathfrak{R}^{r,r}$, an optimal gain matrix $G(t)$ and set of MPFs (contained in α, β) may be determined through the maximization of the performance index

$$\mathcal{J} = \int_0^{t_f} [x_a' Q x_a] \, dt, \qquad Q \triangleq \begin{bmatrix} 0 & 0 \\ 0 & \bar{Q}' \alpha G \beta' \bar{Q} \end{bmatrix} \qquad (40)$$

subject to Eq. (38). Since the optimal solution is stable, $\alpha G \beta'$ is PSD and stability robustness is assessed through sensitivity of its PSD character to perturbations in α and β. If $\alpha = \beta$ (case 4, Table 2), then stability robustness is ensured a priori. Enforcing that $\alpha = \beta$, however, will inevitably lead to an optimal value of the performance index that will be less than the value obtained via the case 3 optimization (hence less effective control) since fewer parameters are allowed in the optimization.

3.   Parameter Optimization via Response to Initial Conditions

A parameter optimization process may be used to determine an SMC design based on a case 3 (Table 2) scenario that is optimal with respect to a given set of initial conditions. For simplicity let G be a constant matrix and consider the following objective function to be minimized subject to Eq. (38):

$$\mathcal{J} = \int_0^\infty (x_a' Q x_a + V' R V) \, dt, \qquad \begin{array}{l} Q \in \mathfrak{R}^{2r, 2r} \\ R \in \mathfrak{R}^{p,p} \end{array} \qquad (41)$$

where Q and R are arbitrarily specified PSD symmetric weighting matrices. Defining $C_0 \triangleq [0 \quad -\beta']$, then since $V = -Gi = -GC_0 x_a$,

$$\mathcal{J} = \int_0^\infty x_a'(Q + C_0' G' R G C_0) x_a \, dt \qquad (42)$$

Equation (42) may be recast in the form[12]

$$\mathcal{J} = x_a'(0) P x_a(0) \qquad (43)$$

where $P \in \mathfrak{R}^{2r, 2r}$ is the solution to the Lyapunov equation

$$A_a' P + P A_a = -(Q + C_0' G' R G C_0) \qquad (44)$$

It is obvious from Eq. (43) that the resultant solution is only optimal with respect to a given set of initial conditions. If the initial conditions typify expected operating conditions, then the resultant design is likely, in general, to perform well. Dependence on initial conditions could be eliminated altogether, if so desired, using the average performance function approach proposed by Levine and Athans.[13] Stability robustness of the (case 3) design must be assessed as discussed earlier. As before, if a case 4 scenario is imposed such that $\alpha = \beta$, then the optimization yields a design for which stability robustness is essentially guaranteed but that is likely to be less effective than the optimal case 3 solution.

4.   Eigenvalue Selection

Again returning to the general linear (case 3, Table 2) scenario, the performance objective now considered is to find α, β, and G to

move the open-loop poles as close as possible to a specified set of desired locations. Defining

$$p(A_a) \triangleq [p_1 \cdots p_{2r}]' \tag{45}$$

$$p_0 \triangleq [(p_1)_0 \cdots (p_{2r})_0]' \tag{46}$$

where p_j is the jth (possibly complex) pole location of A_a and $(p_j)_0$ is the desired jth pole location, then the performance objective may be realized through the minimization of

$$\mathcal{J} = (p - p_0)' Q (p - p_0) \tag{47}$$

subject to Eq. (38), where $Q \in \Re^{2r,2r}$ is a PSD symmetric weighting matrix.

5. Independent Modal Space Control Method Realization

As a final example, a distributed linear realization of the well-known independent modal space control method[14] is sought, in which the control effort is directed entirely toward selectively (and even dynamically) altering the eigenvalue locations of the closed-loop system. A case 4 (Table 2) scenario is assumed. Moreover, $q = p = r$ so that $\alpha \in \Re^{r,r}$ and is a diagonal matrix. A control law of the form $V = -\mathcal{G}i$ is assumed, where $\mathcal{G}$ is a linear operator defined as

$$\mathcal{G} \triangleq \begin{bmatrix} c_1(t) + k_1(t) \displaystyle\int_0^t (\,) \,\mathrm{d}\zeta & & 0 \\ & \ddots & \\ 0 & & c_r(t) + k_r(t) \displaystyle\int_0^t (\,) \,\mathrm{d}\zeta \end{bmatrix} \tag{48}$$

and $c_m(t)$ and $k_m(t)$ are arbitrarily specified scalar functions associated with the mth mode ($m \in R$). The control law is thus an implementation of r distinct proportional-plus-integral control sublaws. The system is assumed to be initially at rest. Then, upon integration, the closed-loop system equations [Eq. (38)] may be reduced and rendered in the form of an r-dimensional set of second-order linear differential equations such that for all $m \in [1, \ldots, r]$

$$\ddot{q}_m + \left[b_0 + c_0\lambda + c_m(t)\alpha_m^2\lambda_m^2\right]\dot{q}_m + \left[\lambda_m + k_m(t)\alpha_m^2\lambda_m^2\right]q_m = 0 \tag{49}$$

Consequently, the character of the controlled system may be varied arbitrarily and dynamically via the functions $c_m(t)$ and $k_m(t)$. Realize, nonetheless, that r SMTs are required and that stability is not necessarily ensured with respect to perturbations in α. Hence, the general design is not stability robust although special forms of the control law are, for example, if all $k_m(t) = 0$ and $c_m(t) \geq 0$.

IV. Numerical Example

A numerical example is now given that serves both to illustrate the SMC design process and to verify the analytical results developed. A general design procedure is identified and then implemented to arrive at an SMC design capable of providing stability robust control for the first six modes of an anisotropic plate. A parameter optimization process is used to derive a suitable set of MPFs and a control law. Implementation is realized via a single SSMA. The SMC design is then validated through numerical simulation.

A. Step 1: Structural Design

As already described, the first step in the design process is to determine the structural design of the composite plate so as to satisfy any mechanical requirements. In this example problem the structural requirements are assumed to warrant the geometry given in Fig. 2. A laminated composite structure is considered in which three mechanically isotropic and piezoelectrically biaxial PVDF layers are bonded to each surface of a double-layered graphite-epoxy composite substrate. Thus, only a single SMT will be implemented. The layers are sequentially numbered from top to bottom (the top layer is referred to as layer 1 and the bottom layer as layer 8). Relevant material properties are given in Table 3, where E_{11}, E_{22}, G_{12}, ν,

Table 3   Example structure material properties

Property	PVDF	G-epoxy
E_{11}, Pa	2.00×10^9	14.5×10^9
E_{22}, Pa	2.00×10^9	9.60×10^9
G_{12}, Pa	1.42×10^9	4.10×10^9
ν_{12}	0.3	0.3
ρ, kg/m^3	1780	1551
$(e_{31}^0)_{\theta=0\,\mathrm{deg}}$ (C/m^2)	60×10^3	——
$(e_{32}^0)_{\theta=0\,\mathrm{deg}}$ (C/m^2)	20×10^3	——

Table 4   Sublaminae skew angles and thicknesses

Layer	1	2	3	4	5	6	7	8
Skew angle, deg	60	0	−60	45	−45	−60	0	60
Thickness, μm	28	28	28	140	140	28	28	28

Table 5   Damping coefficients and natural frequencies

| Mode	Open loop ζ_m,%	Open loop ω_m, rad/s	Ideal closed loop ζ_m,%	Ideal closed loop ω_m, rad/s	Actual closed loop ζ_m,%	Actual closed loop ω_m, rad/s
1	0.057	2.191	99.98	2.709	99.85	2.712
2	0.237	9.475	32.67	8.660	32.51	8.653
3	0.376	13.49	6.308	12.53	6.168	12.58
4	0.764	30.58	8.436	29.86	8.421	29.87
5	0.937	37.49	2.292	37.16	2.176	37.48
6	1.442	57.67	5.569	56.78	5.461	56.32
7	1.548	65.91	1.548	65.91	1.532	65.94
8	1.831	73.26	1.831	73.26	1.827	73.23
9	1.980	79.23	1.980	79.23	1.878	78.91
10	2.348	93.94	2.348	93.94	2.452	94.05
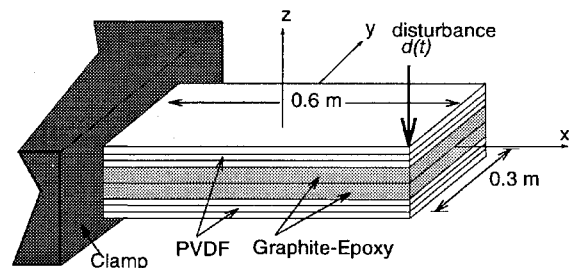
Fig. 2   Example problem geometry.

and ρ refer to the (two) principal stiffness moduli, bulk modulus, Poisson ratio, and volume density, respectively. Laminae skew angles (θ_k defined in Fig. 1) and thicknesses are given in Table 4. The asymmetric layup of the substrate (layers 4 and 5) cause the structure to behave anisotropically. PVDF sublaminae skew angles and thickness were chosen so as to satisfy all SMT construct conditions (Theorem 1, Part 1). Moreover, $-60/0/60$-deg piezolaminae skew angle groupings were chosen so as to ensure that the matrix $E_0 \triangleq \sum_{k=1}^3 e_*^k (e_*^k)'$ is well conditioned (see Appendix A, Part 1).

B. Step 2: Model Generation

A discrete model for the passive system is now developed. The ANSYS finite element modeling (FEM) package[15] was used to generate mass and stiffness matrices (M and K) based on a 169 node finite element representation of the plate. Viscous and structural damping losses were added to the model by introducing a damping matrix C such that $C = b_0 I + c_0 K$, where $[b_0, c_0] = [0.0001, 0.0005]$. The first six mode shapes are given in Fig. 3. Stretching–bending coupling is prevalent, as expected. The first 10 (open-loop) natural frequencies (the mth such natural frequency, $\omega_m = \sqrt{\lambda_m}$) and damping ratios ($\zeta_m$) are listed in Table 5. For the purpose of demonstrating the design procedure and validating the major theoretical findings, both the open-loop natural frequency predictions given in Table 5 and nodal displacement data given in Fig. 3 are assumed to be perfectly accurate.
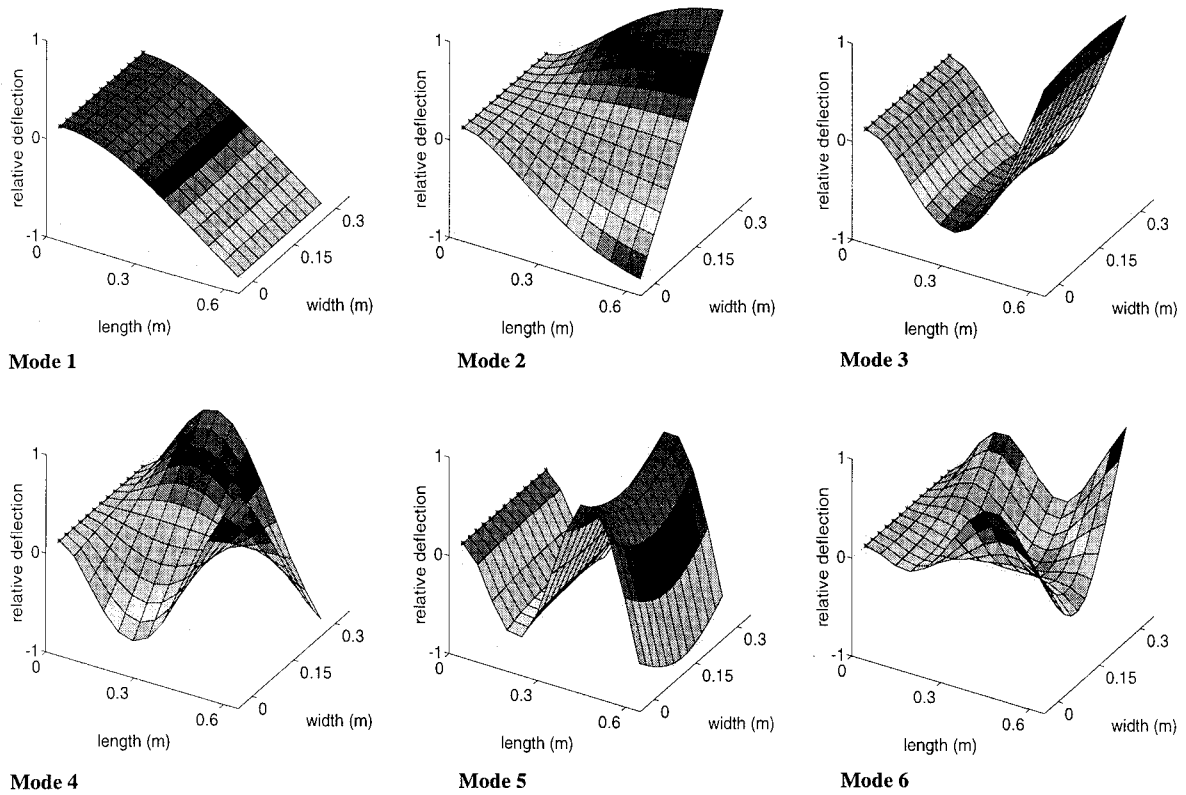
Fig. 3 First six structural modeshapes (deflections are scaled); starred boundary indicates a clamped condition.

C. Step 3: Performance Objective

In this particular example the structure is expected to be excited initially through an impulsive disturbance force $[d(t)]$ acting at a free corner, as shown in Fig. 2. The performance objective is to optimize the system response to the specified excitation using a linear feedback law while excluding from the analysis all modes with natural frequencies above 60 rad/s. To realize the objective, the approach of Sec. III.C.3 is selected. The targeted modal subset is limited to the first six structural modes, as higher modes exceed the specified bandwidth. Equation (38) is thus obtained, where the (open-loop) state matrix, $A \in \Re^{12,12}$, is in the form specified in Eq. (18). Defining $\alpha \triangleq [\alpha_1\lambda_1, \ldots, \alpha_6\lambda_6]$, then

$$\alpha G \beta' = G\alpha\alpha' \qquad (50)$$

where G is the gain constant. To minimize Eq. (41) with respect to α and G, the impulsive force is modeled as a unitary initial displacement acting at the specified location that is resolved via the FEM model into the initial condition position vector

$$q_a(0) =$$

$$[0.2816 \quad -0.3937 \quad -0.2713 \quad 0.4520 \quad 0.2182 \quad -0.6635]'$$

$$(51)$$

to be used in Eq. (43). For the sake of demonstrating and validating the methodology at hand, Eq. (51) is considered perfectly accurate. The weighting matrix, Q in Eq. (41), was selected so as to penalize each mode in inverse proportion to its associated damping coefficient: lightly damped modes are thus penalized more severely. In particular, $Q(j, j), Q(j + 6, j + 6) = \zeta_6/\zeta_j$ for $j = [1, \ldots, 6]$, and all other elements of Q are zero. The control effort is penalized through setting $R \in \Re^1$ to 1. Carrying out the minimization yields as optimal values

$$(\alpha_1, \ldots, \alpha_6, G) = (0.2511, 0.01495, 0.006281, 0.001479,$$

$$0.0005305, 0.0004385, 1.59)$$

Figure 4 describes how the pole locations of the open-loop system [Eq. (18)] are moved in the complex plane when the optimal MPF values are assumed and the feedback gain G is allowed to
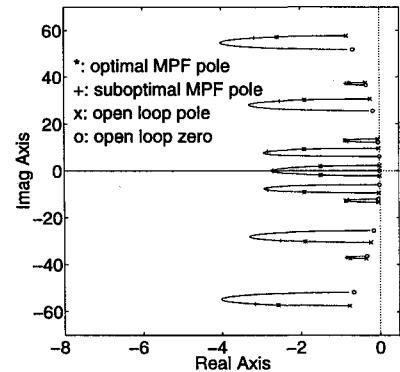

Fig. 4 System root locus for different values of G using optimal MPF values.

vary. The closed-loop pole locations at the optimal gain value are marked in the figure with an asterisk. Although damping is substantially enhanced, it is noted that if $G = 2.482$, then much greater modal damping is realized (as indicated by the plus + points on the plot), whereas the cost functional increases only slightly (from a minimum value of 1.729 to a value of 1.896, whereas in the passive case $J = 497.06$). It is, therefore, decided to implement a final design using the suboptimal $G = 2.482$ value. Open-and closed-loop damping coefficients and natural frequencies that are determined directly from the obtained (complex) pole locations are listed in Table 5 as the ideal values (middle columns). To provide a basis for validating the methodology, these values are considered perfectly accurate: computational errors in the minimization are deemed negligible, and the modeling process has been considered ideal.

D. Step 4: Laminae Piezofield Functions

Having determined the targeted subsystem mode shapes and MPFs, the SSMA design is brought to completion through implementing the piezoelectric field distribution function algorithm [Eq. (30), Part 1],

$$\Lambda^k = \left(1/g_0^k\right)\left(e_0^k\right)' R^{-1} K_a \, \mathcal{E}\bar{\phi}(x, y) \qquad (52)$$

Layer 1   Layer 2   Layer 3
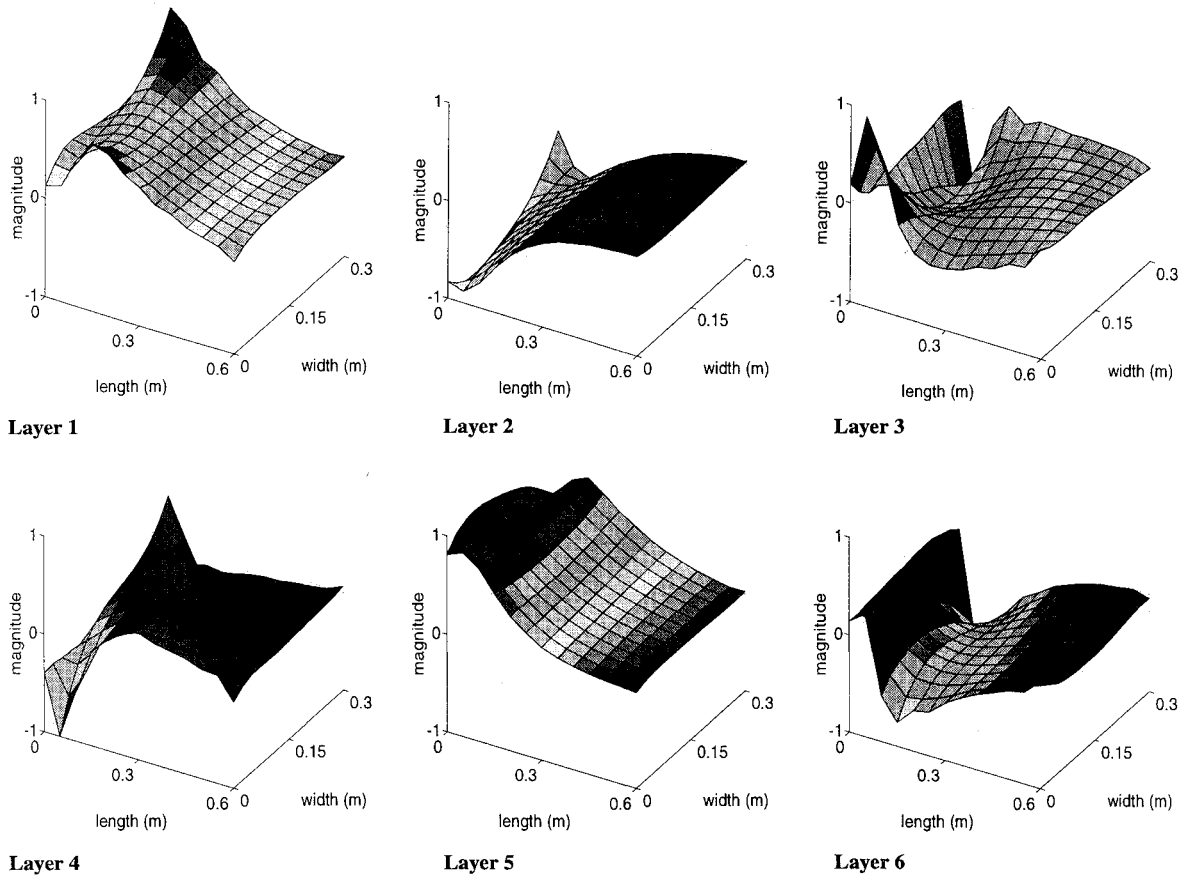
Layer 4   Layer 5   Layer 6

Fig. 5 Piezofield functions for the six SSMA sublaminae.

where the scaling factors $g_0^k \forall k \in [1, \ldots, 6]$, modal subset function $\bar{\phi}$ and matrix R are defined as

$$g_0^k \triangleq \max_{(x,y) \in A} \left| (e_0^k)' R^{-1} K_a \mathcal{E}\bar{\phi}(x, y) \right|, \quad k \in [1, \ldots, 6] \quad (53)$$

$$\bar{\phi} \triangleq \sum_{j=1}^{6} \alpha_j \phi_j \quad (54)$$

$$R \triangleq \sum_{k=1}^{6} e_0^k (e_0^k)' \quad (55)$$

Based on the optimal MPF values and data given in Tables 4 and 5, field function descriptions for each active layer is then determined via numerically approximating Eq. (52) and are shown in Fig. 5. The corresponding set of scaling factors g_0^k for layers 1–6 were found to be 40.67, 102.13, 28.52, 35.00, 102.04, and 29.21, respectively. The numerical approximation of Eq. (52) gives rise to computational errors, which are addressed in the next section.

E. Validation

Having completed the design process, the SSMA design and SMC control law would normally be implemented on the actual structure. For the sake of verifying both the SSMA theory given in Part 1 and the SMC results here, actual structural implementation is replaced here with a numerical simulation. Premultiplying the plate equation of motion [Eq. (1)] by ρh and recalling that $V^k(t) = g_0^k V_a(t)$ such that

$$\rho h x_{tt} + \rho h C x_t + \rho h \mathcal{K} x = -\left[\mathcal{D}' \left(\sum_{k=1}^{N} g_0^k e_0^k \Lambda^k \right) \right] V_a \quad (56)$$

the FEM model (step 1) was derived by ignoring the RHS and discretizing the left-hand side of Eq. (56) to arrive at a numerical model in the form

$$M\ddot{x} + C\dot{x} + Kx = 0 \quad (57)$$

where x is a time-dependent vector of x, y, z displacements at each node location. Using the piezofield functions just determined and including the disturbance force $[d(t)]$, the state equations are augmented through the discretization of the RHS of Eq. (56),

$$M\ddot{x} + C\dot{x} + Kx = fV_a + dd(t) \quad (58)$$

where d is a unit vector whose only nonzero element corresponds to the z translation of the single node at which the disturbance is applied (see Fig. 2). Then, limiting the number of modes of interest to 20 for the purpose of simulation, a modal transformation of the form $x = Vq$ was performed on Eq. (58), where V is a matrix whose columns are the first 20 eigenvectors of Eq. (58) and q is a 20-element column vector containing the first 20 modal coordinates. The modal system representation is then given as

$$\ddot{q} + \bar{C}\dot{q} + \bar{K}q = f_q V_a(t) + d_q d(t) \quad (59)$$

where $\bar{C}$ and $\bar{K}$ are diagonal matrices whose respective elements contain the terms $b_0 + c_0\lambda_m$ and λ_m. The elements of f_q were observed to be very nearly equal to $\alpha_m\lambda_m$, although numerical differentiation gave rise to marginal errors. In particular, the closed-loop damping and natural frequency data that were obtained through Eq. (59) are listed as the actual values in Table 5. The actual values compare favorably with the listed ideal values, which are those values that assumedly would have been obtained if there were no numerical errors. Note that modes 7–10, which are outside the targeted modal subset, are virtually not influenced through active control since the SMTs function as predicted. It is reasonable to assume that discrepancies between the ideal and actual natural frequency estimates in Table 5, which never exceed 0.5%, may be entirely attributed to errors inherent to the numerical approximation of Eq. 52 and the discretization of the RHS of Eq. (56).

To facilitate a performance analysis, a reference measurement $m(t)$ is added whose output is the z displacement of the plate at the point at which the disturbance is applied. Hence, upon conversion

of Eq. (59) to the form of Eq. (18), the augmented system equations are

$$\frac{d}{dt}\begin{bmatrix} q \\ \dot{q} \end{bmatrix} = \begin{bmatrix} 0 & I \\ -\bar{K} & -\bar{C} \end{bmatrix}\begin{bmatrix} q \\ \dot{q} \end{bmatrix} + \begin{bmatrix} 0 \\ f_q \end{bmatrix} V_a + \begin{bmatrix} 0 \\ d_q \end{bmatrix} d \quad (60)$$

$$\begin{bmatrix} i \\ m \end{bmatrix} = \begin{bmatrix} 0 & f'_q \\ d'_q & 0 \end{bmatrix}\begin{bmatrix} q \\ \dot{q} \end{bmatrix} \quad (61)$$

where $i(t) \triangleq (1/\rho h)i_s(t)$. The required feedback law is then

$$V_a = [-G \quad 0]\begin{bmatrix} i \\ m \end{bmatrix} \quad (62)$$

Open- and closed-loop frequency and transient response analyses were computed using the preceding system description. The Bode magnitude and phase plots of the transfer function $m(s)/d(s)$ are given in Fig. 6. Solid lines refer to the passive system response, whereas dashed lines indicate the active system response. Figure 6 shows substantial closed-loop attenuation of the first six modes, whereas all higher order modes remain essentially unaffected. In computing the transient response given in Fig. 7, a unit impulse disturbance was applied through $d(t)$ and the transient response as measured through the reference measurement $m(t)$ was recorded. The closed-loop transient response is extremely rapid. The results
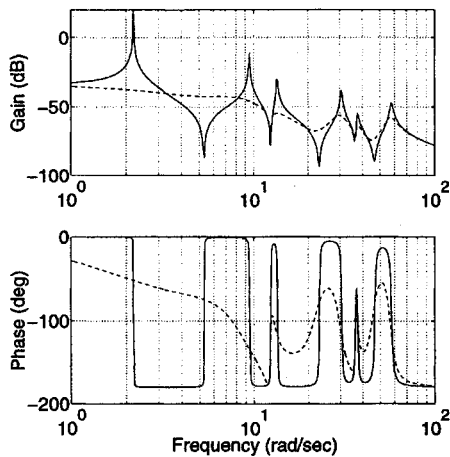

Fig. 6　Frequency response of $m(s)/d(s)$; solid and dashed lines indicate open- and closed-loop response, respectively.
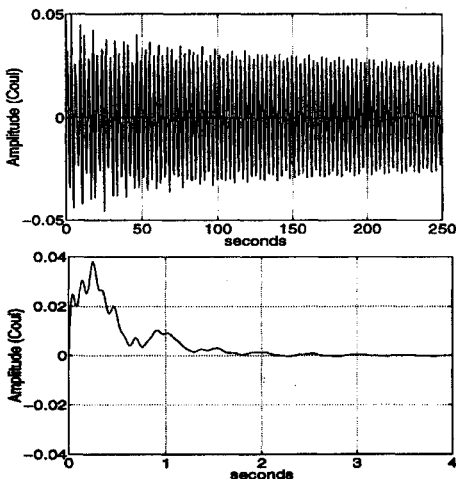

Fig. 7　System response to an impulse disturbance $d(t)$; (top) open loop impulse response, $m(t)$ and (bottom) closed loop impulse response, $m(t)$.

validate the SMC design approach as an effective means of realizing a specified performance objective.

V.　Conclusions

A general design procedure for the realization of SMC has been presented for piezolaminated anisotropic plate systems. General stability criteria were established from which stability robust SMC approaches may be derived. Several representative objective functions were given in which 1) the contributions of any given mode to the active energy extraction rate are directly specified, 2) the closed-loop pole locations are selectively and dynamically assigned, or else 3) eigenvalue locations and SMT design parameters are optimally determined. Most of the listed performance objectives were shown to be realizable through stability robust SMC implementations requiring only a single SMT and proportional feedback. The design procedure was demonstrated through a numerical example in which an SMC method for a composite piezolaminated anisotropic plate was developed. The outcome of that procedure, a specific SSMA design and accompanying control law derived through the parameter optimization of a specified objective function, was then validated through numerical simulation. The results of the numerical study were shown to support theoretical conclusions derived in both parts of this study. Transient and frequency response analyses illustrated a profound improvement in system performance via the SMC approach.

References

[1]Bailey, T., and Hubbard, J., "Distributed Piezoelectric Polymer Active Vibration Control of a Cantilever Beam," *Journal of Guidance, Control, and Dynamics*, Vol. 8, No. 5, 1985, pp. 605–611.

[2]Burke, S., and Hubbard, J. E., "Distributed Actuator Control Design for Flexible Beams," *Automatica*, Vol. 24, No. 5, 1988, pp. 619–627.

[3]Miller, S. E., and Hubbard, J. E., "Smart Components for Structural Vibration Control," *Proceedings of the 1988 American Controls Conference*, Vol. 3, Inst. of Electrical and Electronic Engineers, New York, 1988, pp. 1897–1902.

[4]Burke, S. E., and Hubbard, J. E., "Distributed Transducer Control Design for Thin Plates," *Conference on Electro-Optical Materials for Switches, Coatings, Sensor Optics, and Detectors (SPIE)*, Vol. 1307, Society of Photo-Optical Instrumentation Engineers, Bellingham, WA, 1990, pp. 222–231.

[5]Lee, C. K., "Theory of Laminated Piezoelectric Plates for the Design of Distributed Sensors and Actuators. Part 1: Governing Equations and Reciprocal Relationships," *Journal of the Acoustical Society of America*, Vol. 87, No. 3, 1990, pp. 1144–1158.

[6]Miller, S., Abramovich, H., and Oshman, Y., "Active Distributed Vibration Control of Anisotropic Piezoelectric Laminated Plates," *Journal of Sound and Vibration*, Vol. 183, No. 5, 1995, pp. 797–817.

[7]Miller, S. E., Oshman, Y., and Abramovich, H., "Modal Control of Piezolaminated Anisotropic Rectangular Plates Part 1: Modal Transducer Theory," *AIAA Journal* (to be published).

[8]Dosch, J., and Inman, D., "A Self-Sensing Piezoelectric Actuator for Collocated Control," *Journal of Intelligent Materials and Structures*, Vol. 3, Jan. 1992, pp. 166–185.

[9]Anderson, E. H., Hagood, N. W., and Goodcliffe, J. M., "Self-Sensing Piezoelectric Actuation: Analysis and Application to Controlled Structures," *Proceedings of the AIAA 33rd Structures, Structural Dynamics, and Materials Conference* (Dallas, TX), AIAA, Washington, DC, 1992, pp. 2141–2155 (AIAA Paper 92-2465).

[10]Ashton, J. E., and Whitney, J. M., *Theory of Laminated Plates*, Progress in Material Science Series, Vol. 4, Technomic, Stamford, CT, 1970, pp. 31–42.

[11]Horn, R. A., and Johnson, C. A., *Matrix Analysis*, Cambridge Univ. Press, Cambridge, England, UK, 1985, pp. 61, 62.

[12]Ogata, K., *Modern Control Engineering*, Prentice-Hall, Englewood Cliffs, NJ, 1970, pp. 779–786.

[13]Levine, W. S., and Athans, M., "On the Determination of the Optimal Constant Output Feedback Gains for Linear Multivariable Systems," *IEEE Transaction of Automatic Control*, Vol. AC-15, No. 1, 1970, pp. 44–48.

[14]Meirovitch, L., *Dynamics and Control of Structures*, Wiley, New York, 1990, p. 310.

[15]Anon., "ANSYS Dynamic User Guide for Revision 5.0," Swanson Analysis Systems, Houston, PA, 1993.